High Frequency Passive Microwave Radiometry over a Snow-Covered Surface in Alaska

A.B. Tait, D.K. Hall, J.L. Foster, and A.T.C Chang

Abstract

Millimeter-wave Imaging Radiometer (MIR) data (ranging in frequency from 89 to 325 GHz) were collected from NASA ER-2 flights over Alaska in April 1995. This study determines whether these data can be used to identify clouds, vegetation type, and snow cover. The procedure used is as follows: (1) determine whether a purely MIR-based cloud detection scheme is possible over a snow-covered surface, (2) analyze the influence of changing vegetation type on the brightness temperatures, and (3) compare completely snow-covered scenes with partially snow-covered and snow-free regions for cloudy and clear-sky periods to determine whether varying snow conditions affect the MIR data.

Results show that surface features can be identified using the less opaque channels at 89, 150, and 220 GHz, although the 150-GHz (2.0-mm wavelength) and 220-GHz (1.4-mm) channels are more sensitive to atmospheric phenomena compared with 89 GHz (3.4 mm), because the atmospheric contribution to the upwelling radiation is larger for shorter wavelengths. Statistical examination of the MIR data shows that the determination of cloudy pixels over a snow-covered surface is not possible using a simple brightness temperature threshold technique. Furthermore, it is concluded that, while no statistical discrimination between specific vegetation classes can be made, significance is obtained when the vegetation is grouped into two classes only, for example, vegetated and barren. It is also shown that the state of the snow cover (complete coverage, melting, or patchy) has a distinct effect on these results.

Introduction

The Millimeter-wave Imaging Radiometer (MIR) records radiation emanating from the surface and atmosphere in nine frequency bands: 89, 150, 183.3 ± 1, 183.3 ± 3, 183.3 ± 7, 220, 325 ± 1, 325 ± 3, and 325 ± 8 GHz. The frequencies were chosen to match those of the Advanced Microwave Sounding Unit-B (AMSU-B) planned for NOAA operational satellites and the Earth Observing System (EOS) platform beginning in 2000. The MIR instrument was developed for atmospheric research, with the three channels centered about 183 and 325 GHz designed to study the atmospheric water vapor profile (Racette *et al.*, 1996). Other channels are less opaque and can provide some information about the surface. At an aircraft altitude of around 20,000 m, the temperature sensitivity of the instrument is ≤ 1 K for all channels, and the pixel size is around 500 by 500 m at the nadir. The MIR instrument has been flown on several NASA ER-2 missions, including in Alaska in April 1995.

Between 31 March and 25 April 1995 the ER-2 flew on eight separate occasions over central to northern Alaska and the Bering Sea. The flight dates were 03, 05, 06, 08, 13, 21, 23, and 24 April. Along with the MIR, the aircraft carried several other instruments, including the Moderate Resolution Imaging Spectroradiometer (MODIS) Airborne Simulator (MAS), the Aerosol Particulate Sampler (APS), the High Resolution Interferometer Sounder (HIS), and the Cloud Lidar System (CLS). The principal mission objective was to use remotely sensed data to map snow and ice and make measurements of first-year and multi-year sea ice.

The surface cover in central Alaska is typically spruce, birch, aspen, mixed forest, and muskeg while mountainous and northern regions are generally classified as either sparsely vegetated, barren, or permanent wetland. Over the period of the campaign, the snow conditions over Alaska varied quite markedly. By 06 April the snowpack in central Alaska was beginning to melt and the cover was patchy by 15 April (Hall *et al.*, in press). In northern Alaska, the snow cover remained continuous throughout April.

MODIS cloud-cover and snow-cover algorithms have been developed and tested using several datasets, including data from the MAS (Ackerman *et al.*, 1997; Klein *et al.*, in press). The cloud-cover and snow-cover products derived from these algorithms were used here for comparison with the MIR brightness temperature data. In addition, vegetation maps derived from a Normalized Difference Vegetation Index (NDVI) using Advanced Very High Resolution Radiometer (AVHRR) 1-km data, referred to as the International Geosphere Biosphere Programme (IGBP) land-cover classification (Belward and Loveland, 1995), were used. There are 17 land-cover categories in this classification, ranging from open water to evergreen needleleaf forests.

Racette *et al.* (1996) conclude that it is possible to detect clouds over water and snow-free land using data from the MIR instrument. However, when the surface is covered with snow, it becomes much more difficult to distinguish between the relatively low brightness temperatures associated with the clouds and the similarly low brightness temperatures associated with a snow cover. Chang *et al.* (1987) explain that relatively high frequency microwave data (e.g., 92 GHz) is extremely sensitive to snow crystal scattering; however, the high frequency data are also sensitive to atmospheric water vapor and clouds (Gasiewski, 1992). The MIR instrument measures mixed polarization signals, rather than horizontal and vertical signals; therefore, polarization ratios or differences cannot be used to discriminate clouds. If horizontal and vertical polarizations were measured, it may be possible

NASA/Goddard Space Flight Center, Code 974, Greenbelt, MD 20771.

A.B. Tait is presently with the Universities Space Research Association, 7501 Forbes Blvd., Seabrook, MD 20706 (atait@glacier.gsfc.nasa.gov).

Photogrammetric Engineering & Remote Sensing, Vol. 65, No. 6, June 1999, pp. 689–695.

0099-1112/99/6506–689$3.00/0

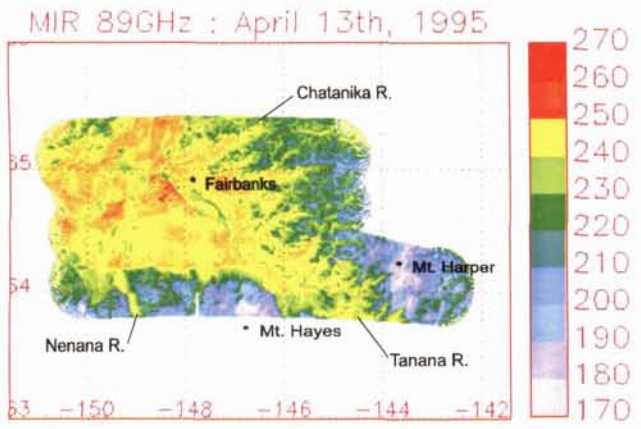

Plate 1. Example of a MIR brightness temperature image over the Fairbanks region of Alaska.

to more readily identify clouds, because surface emissions tend to be polarized while, in general, there is no polarization information from clouds.

Under clear-sky conditions, due to differences in recorded high frequency brightness temperatures between different species of vegetation, Hall *et al.* (1996) suggest that surface vegetation may be detectable. In addition, the MIR data may be used to estimate snow-cover characteristics such as melting snow and snow-covered area. The presence of liquid water transforms a snowpack from one which scatters microwave radiation to one which absorbs and re-emits it (Ulaby and Stiles, 1980). This dramatically increases the brightness temperature (T_B) to that approaching the physical temperature of the medium. Also, Rango *et al.* (1979) show that when the snowpack is dry there is sufficient contrast in the brightness temperature range between snow and bare ground, due to a lower dielectric constant and the effect of scattering in snow, for estimation of snow-covered area.

The objective of this study was to examine the utility of high frequency passive microwave data, recorded by the MIR instrument flown over Alaska in April 1995, for the purpose of identifying clouds over a snow-covered surface, distinguishing differences in vegetation cover, and monitoring snow-covered area. If significant relationships exist, these data may be used to supplement cloud, vegetation, and snow-cover products derived from visible and near-infrared radiation data during periods of low solar illumination or continuous cloud cover. The advantage of using high frequency microwave data for this purpose, compared with lower frequency data, is better spatial resolution. For example, for the Special Sensor Microwave Imager (SSM/I), the resolution at 37 GHz is 37 by 19 km while at 85.5 GHz it is 15 by 13 km.

An Initial Look at the MIR Data

Plate 1 shows a brightness temperature map at 89 GHz for 13 April 1995, for the Fairbanks area in central Alaska. Some of the surface features are clearly visible. The Tanana River can be seen trending southeast from Fairbanks, as can several of the tributaries which flow into it from the mountains to the east and north. The general pattern is of higher brightness temperatures (yellow to red colors) in the lower elevation areas, and lower brightness temperatures (blue to pink colors) at higher elevations. This distinction is a function of the air and surface temperature, presence or absence of snow, and vegetation type and density. Cloud cover may also have an effect on these data. Relationships between the MIR data and these atmospheric and surface phenomena will be investigated in the following sections.

Cloudy Versus Clear Pixels

To test whether clouds can be detected over a snow-covered surface using MIR data, several flight lines from the Alaska mission were analyzed. A multispectral cloud-masking algorithm (Ackerman *et al.*, 1997), derived from MAS data, was used to determine the presence or absence of cloud. Briefly, the cloud-masking algorithm initializes each scene as cloudy and then several threshold tests are performed to determine which pixels are clear. Based on known relationships, cloud type can also be distinguished as either low or high cloud. There are also flags for day or night, sun glint, a snow or ice background, a land or water background, shadow, and an obstructed field of view (by smoke or dust, for example).

Upon visual comparison of MAS-derived cloud-cover maps with the MIR images at 89, 150, and 220 GHz, there is some indication that the presence of clouds has an effect on the microwave data. Surface features typically appear less defined and the brightness temperatures are slightly lower. Figure 1 shows the brightness temperature at 89 GHz for each pixel for the first section of the flight on 03 April 1995. The distance covered on the ground is approximately 3.3 km, and the ground is completely snow covered. The lighter asterisks represent the brightness temperatures of all of the pixels in this section of the data record. There are a total of 18,870 pixels. Plotted over these values is the subset of pixels which has been determined to be cloudy, using the MAS cloud-masking algorithm. These cloudy pixels are delineated as darker crosses, and there are a total of 2,912 pixels, or 15.4 percent of the total number of pixels.

From Figure 1, it appears as though the cloudy pixels generally have lower brightness temperatures than the cloud-free pixels. The number of cloudy pixels was compared with the number of cloud-free pixels using a brightness temperature range between 200 and 220 K, where the majority of the cloudy pixels are located. The total number of cloudy pixels within this brightness temperature range was 2,769. The total number of cloud-free pixels within this range, however, was 12,000. Hence, it appears that, while the brightness temperature of clouds may be lower than some clear-sky pixels, there are a substantial number of clear-sky pixels within the same brightness temperature range. These results were repli-

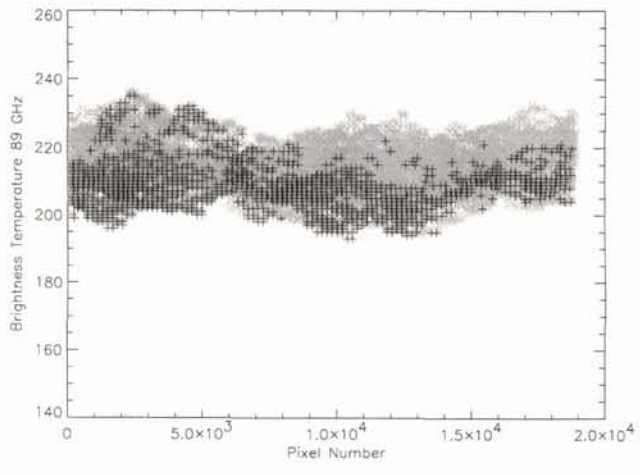

Figure 1. Plot of the first section of data for 03 April 1995. The lighter asterisks are cloud-free pixels and the darker crosses are cloudy pixels.

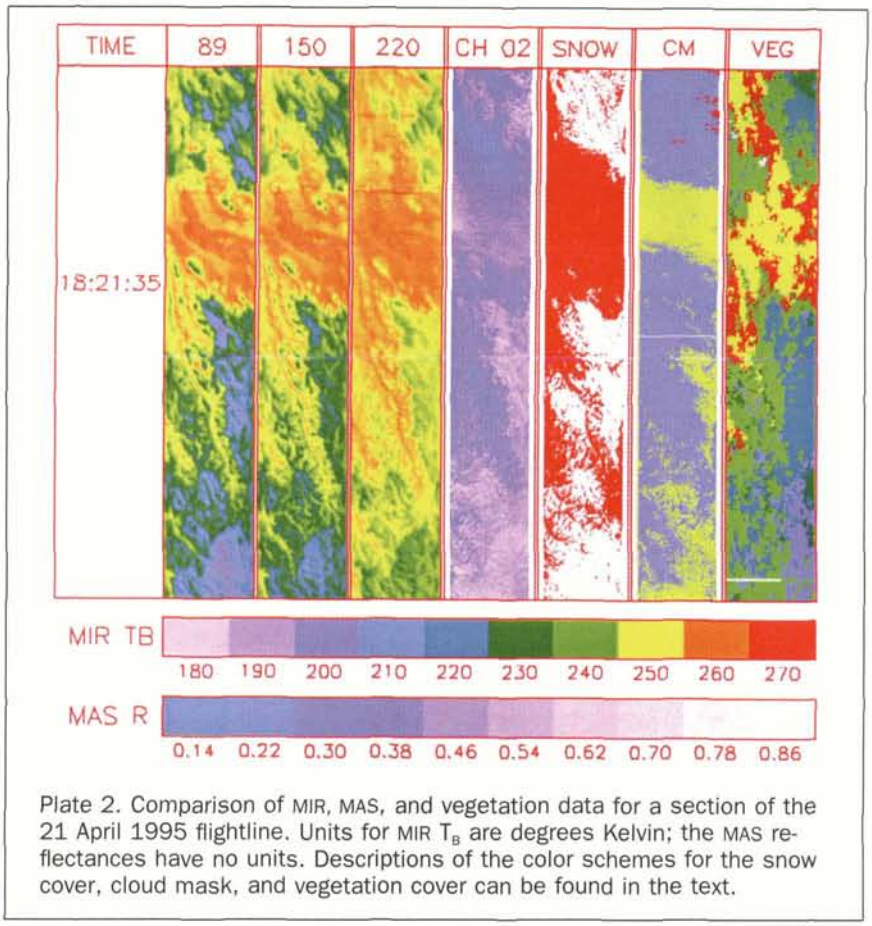

Plate 2. Comparison of MIR, MAS, and vegetation data for a section of the 21 April 1995 flightline. Units for MIR T_B are degrees Kelvin; the MAS reflectances have no units. Descriptions of the color schemes for the snow cover, cloud mask, and vegetation cover can be found in the text.

cated for each of the flights of the Alaska mission, and also for the 150 and 220 GHz channels.

It may be concluded that for these flights over Alaska, while it is possible to visually identify some clouds over a snow-covered surface in an MIR image, it is not possible to discriminate between clouds and clear-sky pixels statistically using the MIR data. This is because while some clouds, particularly low clouds, may be distinguishable from the snow-covered background, the brightness temperature range of all clouds is very similar to that of the snow.

Relationship between Vegetation and Brightness Temperature

Hall *et al.* (1996), using the same Alaskan dataset, conclude that the MIR data show brightness temperature patterns that are related to land cover. They state further that the major delineation appears along the boundary between black spruce forest and the meadow dryas. Coniferous trees emit more microwave radiation than do tundra or dryas vegetation, and this is one explanation for the higher brightness temperatures in the black spruce forests (Hall *et al.*, 1996). These findings were replicated in this study. When looking at images of the brightness temperature data alongside the IGBP vegetation maps (both in the same projection and georeferenced according to latitude and longitude), the boundary between forest and shrubland in the MIR images can often be identified. However, when the brightness temperatures were plotted against the vegetation categories for the 03 April flight for cloud-free pixels only (Figure 2), it was not possible to statistically discriminate between the vegetation categories.

The 03 April flight, though, traversed several degrees of latitude, and the surface maximum air temperature ranged from 10°C (in Fairbanks: 64.5°N) to −14°C (in Prudhoe Bay: 70.4°N). It is possible that these large air temperature differences have masked out any relationship between brightness temperature and vegetation. Therefore, a second flight was analyzed, that of 13 April, which only covered a small area in the Fairbanks region and, hence, had much less of an air temperature range. The results from this analysis, however, were similar to those of 03 April (Figure 3). Using the normalized difference between brightness temperatures at 89 and 150 GHz ([89 − 150]/[89 + 150]) and between 89 and 220 GHz ([89 − 220]/[89 + 220]) as a means of reducing the influence of the air temperature, also resulted in insignificant findings.

Again, as with the cloud analysis, it is concluded that, although changes in the IGBP vegetation type are viewable in the MIR images, statistically significant relationships cannot be determined. This result may be due to the presence of the snow cover. On 03 April snow was continuous over almost all of the flightline. It is possible that the microwave emission and scattering from the snowpack masked the differences caused by different vegetation. Also, as the snowpack was actively melting in central Alaska by 13 April, it is equally possible that the microwave emissions from liquid water, either in the snowpack or in the top layer of soil, confuse the relationship between land-cover type and brightness temperature.

Analysis of a Partially Snow-Covered Scene

Chang *et al.* (1987) conclude that brightness temperature data at 92 GHz can be used to discriminate between snow-covered and snow-free land when clouds are not present. A "first look" of the MIR images from the Alaska 1995 mission verifies this result. Thus, using the MODIS snow-mapping algorithm (Klein *et al.*, in press) on the MAS data to delineate

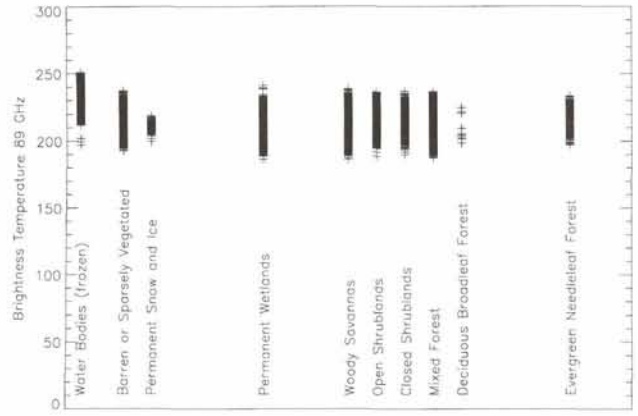

Figure 2. 89-GHz brightness temperature versus IGBP land-cover classes for 03 April 1995.

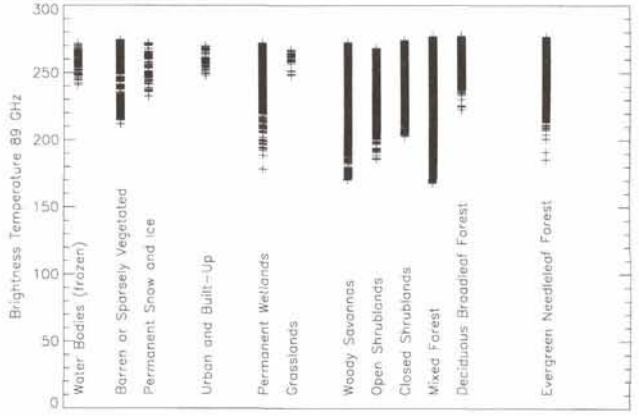

Figure 3. 89-GHz brightness temperature versus IGBP land-cover classes for 13 April 1995.

the snow boundary, and using the MAS cloud-masking algorithm to determine cloud-free pixels only, an analysis of the MIR data for 13 April was performed. This day was chosen because the MODIS snow-mapping algorithm shows patchy snow around the Fairbanks region. Figure 4 shows the same type of plot used to test the relationship between vegetation and brightness temperature. However, in addition to showing the variation between vegetation categories, this plot also separates out snow-free pixels as darker crosses, and snow-covered pixels as lighter asterisks.

From Figure 4 it can be seen that the snow-free pixels have a smaller brightness temperature range for many of the vegetation categories, and have fewer lower brightness temperatures compared with the snow-covered pixels. Lower values were expected over snow-covered areas, because the snow grains scatter the upwelling radiation, causing a reduction in the brightness temperature. The same pattern, though less defined, was obtained using 150- and 220-GHz data. However, there are a significant number of snow-covered pixels in the same brightness temperature range as the snow-free pixels, for many of the vegetation classes (Figure 4). When the brightness temperatures of these snow-covered pixels were compared with the snow-free pixels using a t-test, a statistical differentiation between the two sets could not be accomplished.

Once again, despite some indication that snow-free pixels tend to have higher brightness temperatures, no statistical discrimination is possible. Normalized difference ratios were again used to reduce the influence of the air and surface temperature, but with no improvement in the statistical significance. As previously mentioned, these results may be affected by the presence of liquid water either in the snowpack or in the top layer of the soil. To reduce this problem, future missions may consider nighttime flights when much of the meltwater has re-frozen.

Analysis of a Completely Cloud-Covered Scene

The flight on 21 April 1995 was almost entirely cloud covered. It is during conditions such as this that microwave data should be most useful, to supplement the visible data. Can the vegetation type or the presence of snow cover be detected using the MIR data?

Plate 2 is a side-by-side comparison of MIR, MAS, and IGBP vegetation data for a section of the 21 April flightline. The first three columns represent plots of the data from the 89-, 150-, and 220-GHz channels of the MIR instrument. There is an overall increase in the brightness temperature as the frequency increases. This is due to an increase in the atmospheric contribution to the upwelling radiation with higher frequencies (Schanda and Hofer, 1977). The fourth column is the Channel 2 (0.627-μm) reflectance data from MAS. Note that the width of this and the next two columns is a little less than the MIR data, due to the different scan angles of the instruments (MIR = 100°, MAS = 85.92°). The MIR data and the MAS Channel-2 data are a little blurred due to the presence of the cloud cover. Many surface features are still discernable, however, particularly in the 89-GHz image.

The fifth column depicts the location of snow (in white) as mapped by the MAS snow-mapping algorithm. Because the algorithm is based on optical data, no snow will be mapped under thick cloud cover. The sixth column shows the cloud cover as prescribed by the MAS cloud-masking algorithm. The scene is 100 percent cloud covered. In blue are pixels which have been designated high cloud only, while the yellow pixels represent both high and low clouds and red pixels denote low cloud only. Lastly, the vegetation is mapped. The pixels colored red through dark green are forested (red = evergreen needleleaf; yellow = deciduous broadleaf; dark green = mixed forest). The light green represents closed

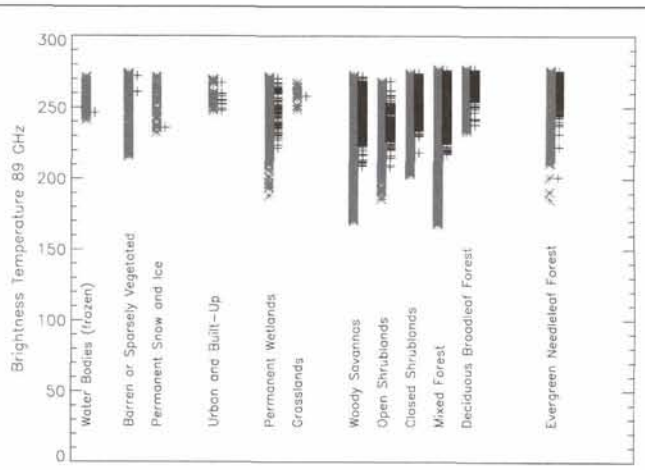

Figure 4. Snow-covered (light asterisks) versus snow-free (dark crosses) pixels for 13 April 1995.

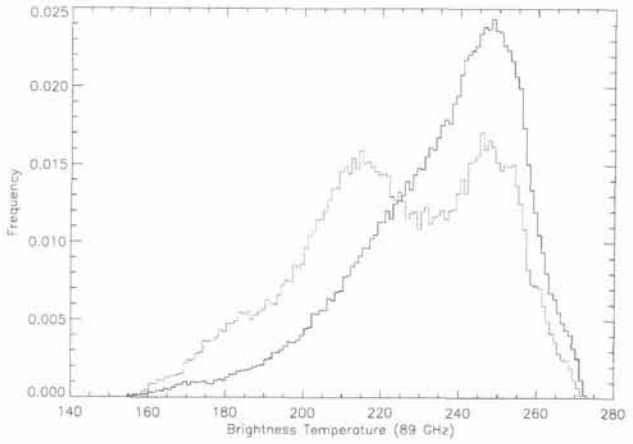

Figure 5. Histograms of forested (solid) and non-forested (dotted) vegetation groups for 21 April 1995.

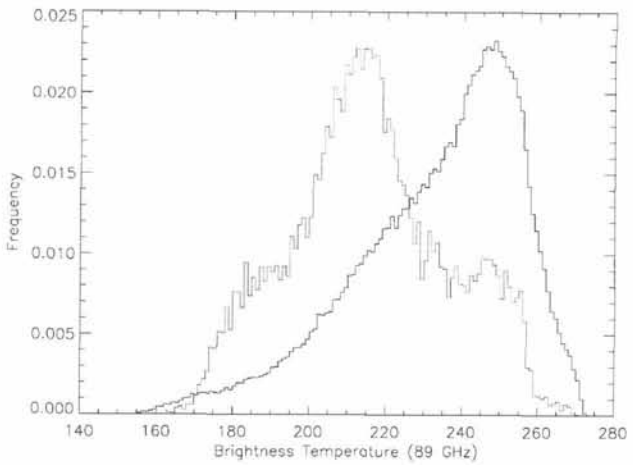

Figure 6. Histograms of vegetated (solid) and barren (dotted) land groups for 21 April 1995.

shrublands and the light blue depicts open shrublands. The purple-colored area is permanent wetland.

There appears to be a distinct relationship between the MIR brightness temperatures, the snow cover, and the vegetation type. It appears as though generally higher brightness temperatures are associated with forested regions with no snow cover, while lower brightness temperatures are related to the snow-covered open areas. When data from the entire flight were analyzed, though, no such relationships could be determined. However, concentrating only on the section of the 21 April flight shown in Plate 2, and grouping all the forest categories together and all the non-forested categories together, the difference between the two groups at all three MIR channels was statistically significant (t-test, significance level $< 0.1\%$). The mean T_B (89 GHz) for the combined forested pixels was 247.6K, while the mean for the non-forested pixels was 234.9K. The differences using the 150- and 220-GHz data were less, but were still statistically significant.

This result suggests that the high frequency MIR data can be used to discriminate between some surface features such as between forest and non-forest, even under cloudy conditions. The following section investigates this result further, by analyzing the entire flightlines of 03, 13, and 21 April.

Analyses of Binary Classifications of Vegetation

Based on the previous result, the MIR brightness temperature data for the entire 21 April 1995 flightline were analyzed by testing for a difference between the means of the forested pixels and the non-forested pixels. The difference using the 89-GHz channel was more significant than the higher frequencies, due to less atmospheric effects. At 89 GHz, the t-test was significant (significance level $< 0.1\%$) with the mean $T_{B(Forest)} = 235.1$K, and the mean $T_{B(Other)} = 223.8$K.

However, Figure 5, which shows the histograms of the two vegetation groups, indicates that the non-forested group is bimodal and that some of the non-forested pixels clearly belong in the forested category. Hence, beginning with "closed shrublands," vegetation classes were systematically removed from the non-forested category and added to the forested category. With every iteration, the second peak in the non-forested histogram decreased while the first peak increased. The best discrimination between brightness temperatures for 21 April is shown as Figure 6, where the solid line represents all vegetated surfaces and the dotted line represents barren land (mean $T_{B(Vegetated)} = 233.5$K (89 GHz), mean $T_{B(Barren)} = 215.7$K (89 GHz)). This result shows that brightness temperature differences are greatest in response to the presence or absence of vegetation, rather than the boundary between, for example, forest and shrublands.

To test this result, data from 13 April and 03 April were analyzed. Figures 7 and 8 represent the histograms of forested versus non-forested, and vegetated versus barren for the 13 April flight. On this day very little discrimination can be made between either of the vegetation groupings. It is argued that this is a direct function of the presence of melting snow. Hall *et al.* (in press) show that there was rapid melting in the Fairbanks region between 06 and 15 April. It is therefore likely that the presence of liquid water in the snowpack is masking the differences in the microwave signal caused by the vegetation.

The histograms for 03 April are shown as Figures 9 and 10. Figure 9, which represents delineation between forests and non-forests, is almost the complete opposite of Figure 5, the same vegetation groupings for 21 April. In Figure 9 it is the forest category which is bimodal, and it is clear that some of these data belong in the non-forested category. Thus, beginning with "mixed forest," the vegetation groups were

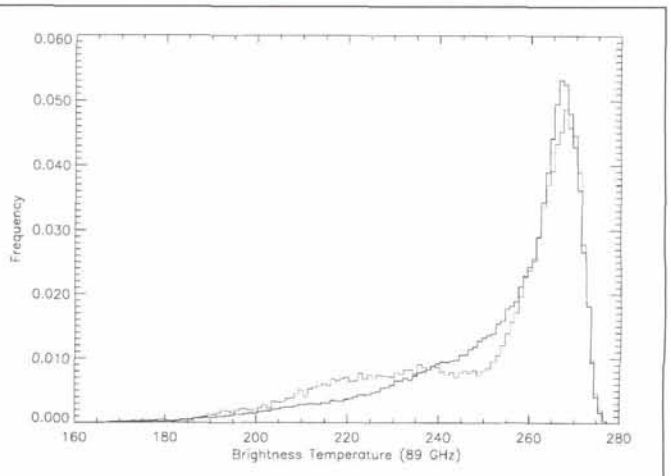

Figure 7. Histograms of forested (solid) and non-forested (dotted) vegetation groups for 13 April 1995.

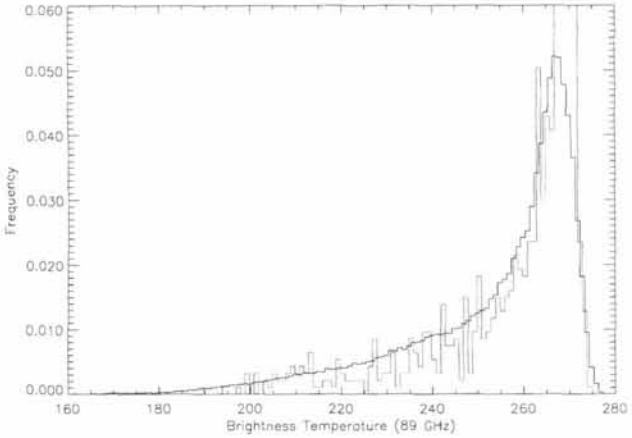

Figure 8. Histograms of vegetated (solid) and barren (dotted) land groups for 13 April 1995.

re-classified by removing classes from the forested class and adding them to the non-forested class. Figure 10 represents the best discrimination between vegetation types. Here, the solid line is evergreen needleleaf forest only and the dotted line is everything else. Despite some overlap between classes, the difference between the two means is highly significant (significance level $< 0.1\%$), with the mean $T_{B(Evergreen)} = 233.8K$ (89 GHz) and the mean $T_{B(Other)} = 222.0K$ (89 GHz).

This result highlights the impact of a continuous dry snow cover and the ability of the MIR instrument to view the snow cover. In all the vegetation classes except evergreen forest, the sensor can detect the presence of snow on the surface, and the scattering from this snow is effectively reducing the brightness temperature. However, the denser canopy of the evergreen forest is able to mask much of the snowpack scattering, in addition to contributing to the relatively warmer brightness temperatures through emission from the trees themselves.

Therefore, the condition of the snowpack is vital in determining the best binary delineation between vegetation types, based on high frequency microwave data. If the surface is almost snow-free, then the MIR data best delineate the boundary between vegetated and barren land. When the snow is melting, the microwave signal is swamped by the presence of liquid water and little discrimination between vegetation types is possible. If a continuous coverage of dry snow is present, then high frequency microwave data can be used to effectively delineate between evergreen trees and other vegetation classes.

Discussion and Conclusions

Previous studies have indicated that high frequency (greater than 80 GHz) microwave data may be useful in the identification of such phenomena as clouds, snow, and vegetation. One of the main difficulties, as this study shows, is the identification of clouds over a snow-covered surface due to very similar brightness temperature values. If the MIR recorded polarized data, then such discriminations may be possible using a polarization ratio or difference. A further consideration for future missions using the ER-2 is a nighttime flight over a patchy snow cover. This may reduce the influence of melting snow on the brightness temperatures and enhance the differences between snow-covered and snow-free land. Satellite-derived microwave maps of snow cover use nighttime orbits to ensure snow is as dry as possible.

Results from this study confirm other reports that vegetation types can be visually identified using high frequency brightness temperature data. However, it is concluded that no statistical relationship is present between brightness temperature and the IGBP land-cover classes; hence, it is not possible to objectively detect such detailed surface features under snow-cover conditions. Alternatively, when the vegetation classes were grouped into binary classifications, highly significant results were produced. This suggests that there is an underlying relationship between brightness temperature and surface features, but that it is only statistically significant when the vegetation groups are simplified.

A major implication of this research concerns the estimation of snow-covered area, snow depth, and snow water equivalent using passive microwave radiation data. It has been shown by several authors (e.g., Chang *et al.*, 1997) that forest cover has a significant effect on brightness temperatures in the range 18 GHz to 37 GHz. Tait (1998) made several land-cover divisions, including forested and unforested, as a means of enhancing the snow-cover signal. This study

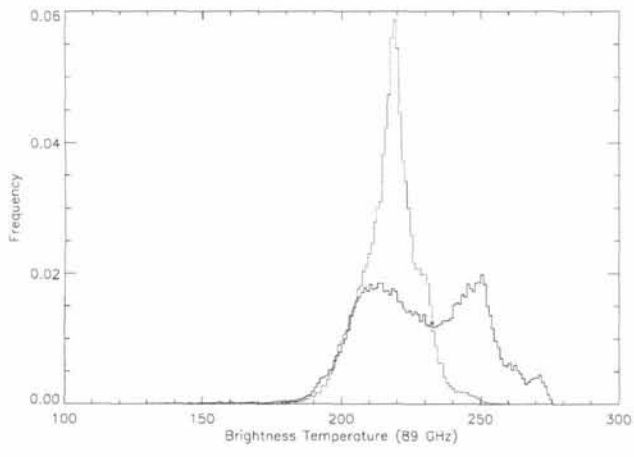

Figure 9. Histograms of forested (solid) and non-forested (dotted) vegetation groups for 03 April 1995.

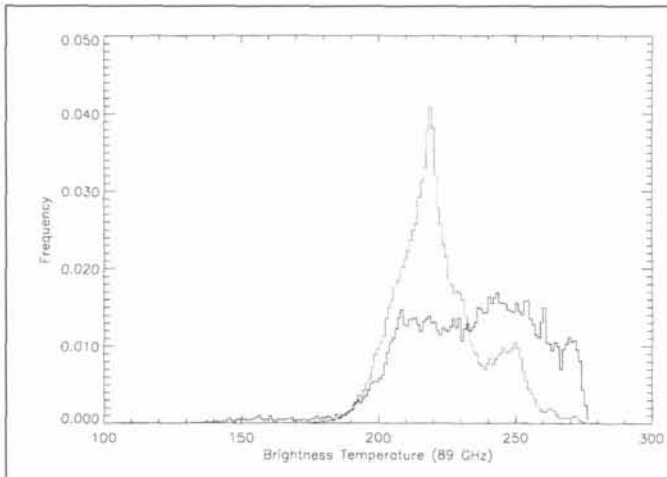

Figure 10. Histograms of evergreen forest (solid) and other (dotted) groups for 03 April 1995.

shows, however, that such a division may not necessarily represent the best binary land-cover delineation. It is shown here that the optimum vegetation discrimination is strongly related to the condition of the snow cover. This should be considered for future studies of passive microwave estimates of the snow cover.

Acknowledgments

The authors wish to thank Carl Benson, Geophysical Institute, University of Alaska, for his help gathering field data, and Jim Wang and Paul Racette, NASA/GSFC, for their help in collecting and calibrating the MIR data. This work is supported by the EOS/MODIS Snow and Ice Project.

References

Ackerman, S., K. Strabala, P. Menzel, R. Frey, C. Moeller, L. Gumley, B. Baum, C. Schaaf, and G. Riggs, 1997. *Discriminating Clear-Sky from Cloud with MODIS. Algorithm Theoretical Basis Document, Version 3.2 (MOD35)*, [publisher, place], 131 p.

Belward, A.S., and T.R. Loveland, 1995. The IGBP-DIS 1km Land Cover Project: Remote sensing in action, *Proceedings of the 21st Annual Conference of the Remote Sensing Society*, Southampton, UK, pp. 1099–1106.

Chang, A.T.C., J.L. Foster, and D.K. Hall, 1987. Microwave snow signatures (1.5mm to 3cm) over Alaska, *Cold Regions Science and Technology*, 13:153–160.

Chang, A.T.C., J.L. Foster, D.K. Hall, B.E. Goodison, A.E. Walker, J.R. Metcalfe, and A. Harby, 1997. Snow parameters derived from microwave measurements during the BOREAS winter field campaign, *Journal of Geophysical Research*, 102(D24):29,663–29,671.

Gasiewski, A.J., 1992. Numerical sensitivity analysis of passive EHF and SMMW channels to tropospheric clouds, water vapor, and precipitation, *IEEE Transactions of Geoscience and Remote Sensing*, 30:859–870.

Hall, D.K., J.L. Foster, A.T.C. Chang, D.J. Cavalieri, and J.R. Wang, 1996. Analysis of snow cover in Alaska using aircraft microwave data (April 1995), *Proceedings of IGARSS 1996*, Lincoln, Nebraska, pp. 2246–2248.

Hall, D.K., J.L. Foster, A.T.C. Chang, C.S. Benson, and J.Y.L. Chien, in press. Determination of snow-covered area in different land covers in central Alaska, U.S.A., from aircraft data - April 1995, *Annals of Glaciology*.

Klein, A.G., D.K. Hall, and G.A. Riggs, in press. Improving snow-cover mapping in forests through the use of a canopy reflectance model, *Hydrological Processes*.

Racette, P., R.F. Adler, J.R. Wang, A.J. Gasiewski, D.M. Jackson, and D.S. Zacharias, 1996. An airborne millimeter-wave imaging radiometer for cloud, precipitation, and atmospheric water vapor studies, *Journal of Atmospheric and Oceanic Technology*, 13(3): 610–619.

Rango, A., A.T.C. Chang, and J.L. Foster, 1979. The utilization of space-borne microwave radiometers for monitoring snowpack properties, *Nordic Hydrology*, 10:25–40.

Schanda, E., and R. Hofer, 1977. Microwave multispectral investigation of snow, *Proc. 11th Int. Symp. Remote Sensing of the Environment*, Environmental Research Institute of Michigan, Ann Arbor, Michigan, pp. 601–607.

Tait, A.B., 1998. Estimation of snow water equivalent using passive microwave radiation data, *Remote Sensing of Environment*, 64: 286–291.

Ulaby, F.T., and W.H. Stiles, 1980. Microwave radiometric observations of snowpacks, NASA CP-2153, *NASA Workshop on the Microwave Remote Sensing of Snowpack Properties*, Ft. Collins, Colorado, 20-22 May, pp. 187–201.

(Received 15 April 1998; accepted 18 August 1998; revised 02 September 1998)